

Personalized Hydrogels for Engineering Diverse Fully Autologous Tissue Implants

Reuven Edri, Idan Gal, Nadav Noor, Tom Harel, Sharon Fleischer, Nofar Adadi, Ori Green, Doron Shabat, Lior Heller, Assaf Shapira, Irit Gat-Viks, Dan Peer, and Tal Dvir*

Despite incremental improvements in the field of tissue engineering, no technology is currently available for producing completely autologous implants where both the cells and the scaffolding material are generated from the patient, and thus do not provoke an immune response that may lead to implant rejection. Here, a new approach is introduced to efficiently engineer any tissue type, which its differentiation cues are known, from one small tissue biopsy. Pieces of omental tissues are extracted from patients and, while the cells are reprogrammed to become induced pluripotent stem cells, the extracellular matrix is processed into an immunologically matching, thermoresponsive hydrogel. Efficient cell differentiation within a large 3D hydrogel is reported, and, as a proof of concept, the generation of functional cardiac, cortical, spinal cord, and adipogenic tissue implants is demonstrated. This versatile bioengineering approach may assist to regenerate any tissue and organ with a minimal risk for immune rejection.

Engineered functional tissue implants have advanced in recent years to address the problem of limited organ donor availability for transplantation. In this approach, 3D biomaterials in the form of scaffolds or injectable hydrogels, encapsulate cells to provide physical support, as well as to provide biochemical and topographical cues for cellular assembly and function. These cells depend heavily on specific properties of the engineered matrix. In addition, depending on the specific characteristics of cell–cell and cell–matrix interactions, extracellular matrix (ECM) proteins are secreted to shape the microenvironment, while the biomaterial degrades.^[1]

Over the years, different types of scaffolds have been used for the regeneration of complex organs, such as the infarcted heart, injured spinal cord, and the neurodegenerative brain. The scaffolds' properties were rationally designed to support cell assembly to a specific desired tissue, without a universal material that fits all.^[1] In principle, these scaffolding materials originate from synthetic or natural sources, or even from decellularized xenogeneic tissues.^[2,3] However, in most of the cases there is an immunological mismatch between the graft and the host tissue.^[4,5] For example, the bulk materials, the degradation products of the fabricated scaffolds, the remaining matrix antigens on decellularized materials or interspecies differences in the sequences of ECM proteins may provoke an adverse immune response following transplantation.^[6,7] Such immunological reaction jeopardizes treatment success and may lead to the rejection of the engineered implant. Therefore, even use of extremely DNA-free decellularized matrices may require immunosuppression throughout the patient's lifetime.^[8]

Where possible, autologous cells are used to eliminate the undesirable immunological effects of cellular components. However, for many diseases, such as cardiac and central nervous system (CNS) diseases, autologous cells are not available. To overcome this therapeutic challenge, induced pluripotent stem cells (iPSCs) are generated from the patient's own

Dr. R. Edri, I. Gal, T. Harel, Dr. S. Fleischer, Dr. A. Shapira, Prof. I. Gat-Viks, Prof. D. Peer, Prof. T. Dvir
School for Molecular Cell Biology and Biotechnology
Tel Aviv University
Tel Aviv 69978, Israel
E-mail: tdvir@post.tau.ac.il

Dr. R. Edri, Prof. D. Peer, Prof. T. Dvir
The Center for Nanoscience and Nanotechnology
Tel Aviv University
Tel Aviv 69978, Israel

N. Noor, N. Adadi, Prof. D. Peer, Prof. T. Dvir
Department of Materials Science and Engineering
Tel Aviv University
Tel Aviv 69978, Israel

O. Green, Prof. D. Shabat
School of Chemistry
Tel Aviv University
Tel Aviv 69978, Israel

Prof. L. Heller
Department of Plastic Surgery
Assaf Harofeh MC
Beer Ya'akov, Zerifin 70300, Israel

Prof. T. Dvir
Sagol School of Neuroscience
Tel Aviv University
Tel Aviv 69978, Israel

Prof. T. Dvir
Sagol Center for Regenerative Biotechnology
Tel Aviv University
Tel Aviv 69978, Israel

 The ORCID identification number(s) for the author(s) of this article can be found under <https://doi.org/10.1002/adma.201803895>.

DOI: 10.1002/adma.201803895

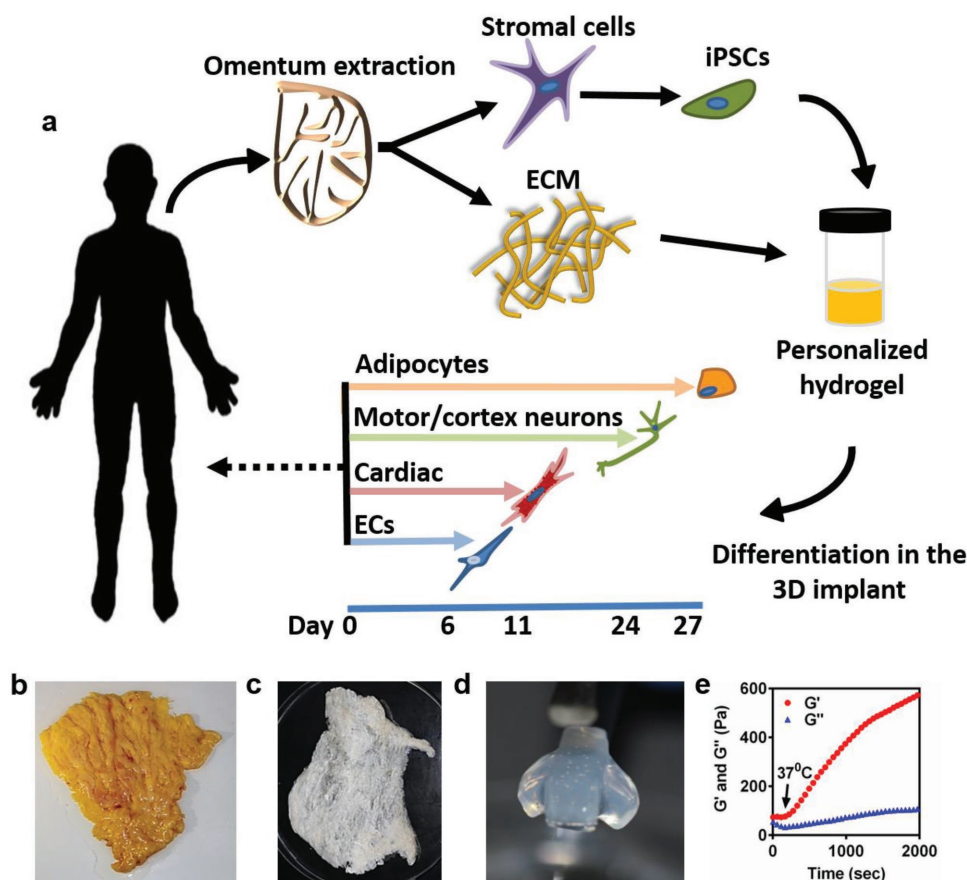


Figure 1. Engineering patient-specific implants. a) Concept schematic. An omentum specimen is extracted from the patient and, while tissue ECM is processed into a personalized thermoresponsive hydrogel, the cells are reprogrammed to become iPSCs. Next, the cells are encapsulated within the hydrogel and efficiently differentiate to various lineages, generating functional tissue implants. b–e) Fabrication of the personalized thermoresponsive hydrogel. (b) Human omentum, extracted from a patient. (c) Decellularized matrix. (d) Omentum hydrogel. (e) Hydrogel rheological measurements showing gelation kinetics at 37 °C.

cells.^[9] After efficient differentiation to the desired cell types, iPSCs can be used for disease models,^[10] drug screening,^[11] and personalized cell therapies.^[12] Currently, iPSCs are cultured as monolayer cellular colonies or in suspension,^[13] with Matrigel (MG) being the most frequently used supporting microenvironment. The cells are then exposed to biomolecules and growth factors to promote proliferation and differentiation. iPSCs can be differentiated as embryoid bodies to form organoids,^[14] which lack a protective microenvironment.^[15] Alternatively, cells can be encapsulated in 3D MG drops.^[16] However, since MG is derived from mouse sarcoma tumors, its safety for use as a support system for cells that will be used for implantation in humans is unconfirmed.^[17]

Here, we introduce a new approach to efficiently engineer any tissue type, which its differentiation cues are known, in a personalized manner by extraction and manipulation of small tissue biopsies from individual patients (Figure 1a). Here, a small piece of the omentum, a highly vascularized fatty tissue, which among other roles serves as a depot for stem cells and has regenerative capabilities,^[18] is extracted from the patient in a safe, easy, and quick procedure.^[19] The cells and the ECM are separated so that the ECM can be processed into a personalized thermoresponsive hydrogel and the cells can be reprogrammed

to become pluripotent. The undifferentiated cells are then homogeneously encapsulated within the 3D hydrogel and as a proof of concept, efficiently differentiated into cardiomyocytes, cortical, and motor neurons, endothelial cells (ECs) or adipocytes in their original environment. The cell-containing hydrogels are then developed into functional tissue implants.

Omentum tissues were extracted from healthy human donors for the proof of concept, or from pigs and decellularized (Figure 1b,c and Figure S1a, Supporting Information). The remaining ECM material was processed using chemicals and enzymes to generate a thermoresponsive hydrogel. The human material-based hydrogel, which was a weak hydrogel at room temperature and was composed of collagen fibers and glycosaminoglycans (Figure S1b, Supporting Information), physically cross-linked under physiological conditions by conformational change of the digested macromolecules and their entanglement^[20,21] (Figure 1d,e; Figure S2, Supporting Information). Such hydrogels did not degrade under *in vitro* conditions.^[22]

We hypothesized that immune response to decellularized xenogeneic materials, such as pigs' matrices, which are widely used in the clinic could be attributed to two main reasons. One may be specific proteins and polysaccharides that cannot be found in humans.^[23] Another reason may be inter-species

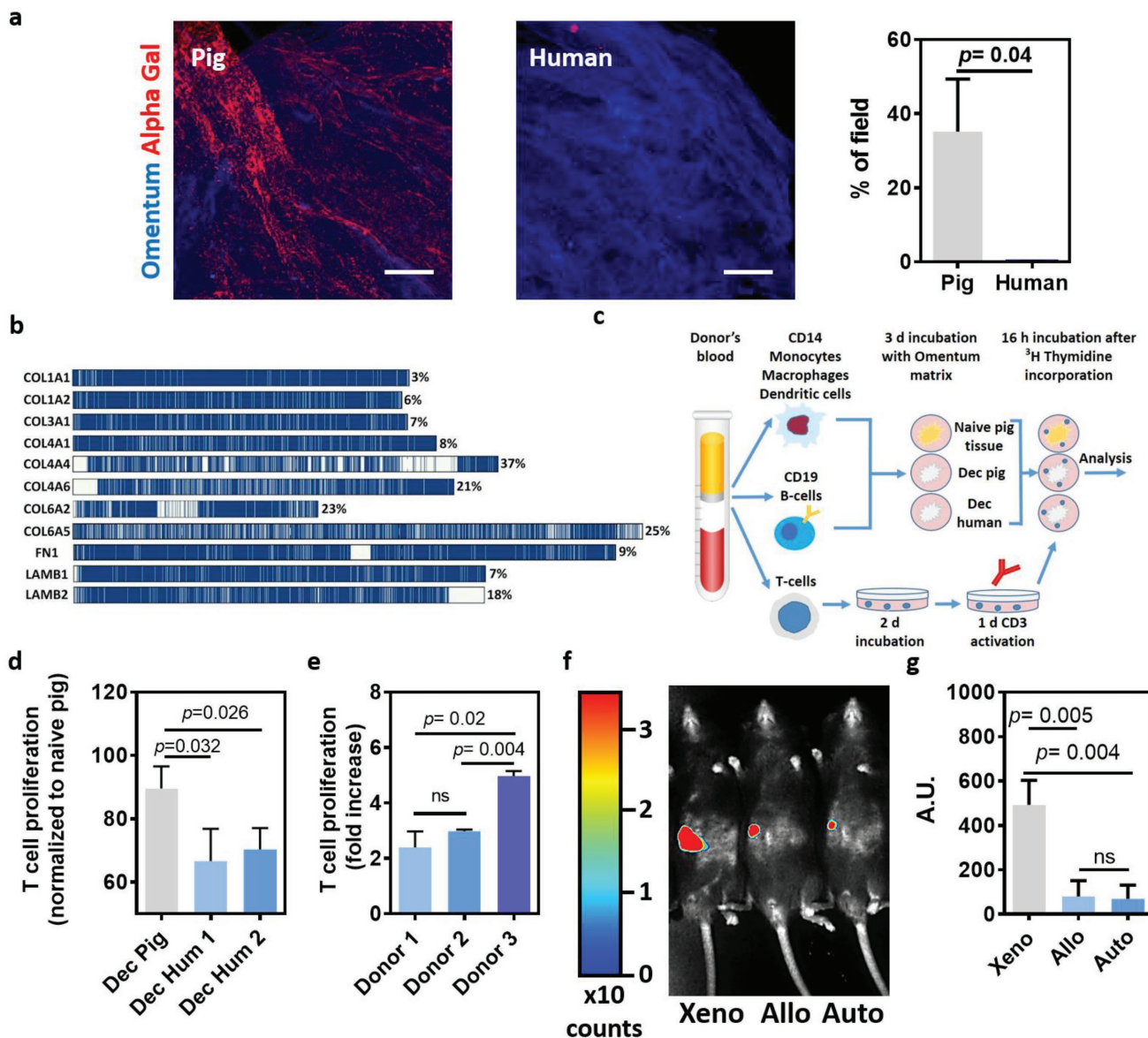


Figure 2. Immune response to autologous materials. a) Immunostaining and quantification of Alpha-Gal epitope (red) in decellularized porcine and human omental tissue (blue). b) Amino acid sequence homology comparison between porcine and human ECM proteins, similarities in sequence are shown in blue, discrepancies in white. Percentage of variation appears on the right. c) Experimental procedure scheme of a human in vitro immune response assay. Donor blood is centrifuged with Ficoll, PBMC are extracted and APCs – monocytes, DCs, macrophages (CD14+) and B-cells (CD19+) are sorted and incubated for 3 days with naive and decellularized porcine and human omental tissues. Remaining T-cells are grown for 2 days, incubated for 1 day with anti-CD3 and comixed with APCs O.N. ^3H -Thymidine is added and the proliferation after 16 h is measured. d) Proliferation of cells of three different patients after exposure to porcine and human decellularized omentum matrices. Values are normalized to these of the cells exposed to naive pig tissue. e) Donor-specific response of different donors. Proliferation is normalized to each individual cell number before exposure to the decellularized tissues. f) In vivo imaging of endogenous ROS in the peritoneal cavity of mice, showing the response to xenogenic, allogeneic and autologous implants, 7 days post transplantation. g) Quantification of signal intensities measured from each group of mice ($n = 3$ for each group).

variations in the amino acid sequence of ECM proteins.^[24] In these cases, after transplantation, antigen-presenting cells (APCs) such as monocytes, dendritic cells (DCs), macrophages, and B cells may recognize these antigens as foreign molecules, and present them to T cells that in turn become activated.^[7] Therefore, we initially sought to demonstrate the presence of such antigens in the xenogeneic decellularized hydrogel. Immunostaining of pig or human-derived hydrogels

against the alpha gal antigen, a carbohydrate found in mammals but not in primates,^[5] revealed a pronounced staining in the pig hydrogel, even after aggressive decellularization steps (Figure 2a). A bioinformatic analysis has shown significant changes between human and pig sequences of important ECM proteins (Figure 2b; Figure S3, Supporting Information). For example, adhesions proteins, such as laminin (LAMB2) and fibronectin (FN1) have amino acid sequence variations of 18%

and 9%, respectively. Structural ECM proteins, such as collagen I (COL1A2) and III (COL3A1) have a sequence variation of more than 6%. Finally, different chains of collagen IV, a protein composing the ECM of blood vessels have a sequence variation between 8% (COL4A1) to 37% (COL4A4). The structural and adhesion proteins are the main proteins in the decellularized matrix, and their preservation during the decellularization process is essential for cell growth. Such variations between the species may trigger an immune response after transplantation.^[7] Since the omentum tissue is rich with blood vessels, a sequence variation in collagen IV, one of the main ECM proteins of the basement membrane may also provoke an immune response.

To evaluate the actual response of human immune cells to pigs' or humans' omentum ECM hydrogels, an *in vitro* assay was performed (Figure 2c and the Experimental Section). Blood was collected from three donors and APCs (monocytes, DCs, and macrophages) together with B cells and T cells were isolated. The APCs were exposed for 72 h to pigs' and humans' digested decellularized tissues, and to naïve pig tissue (positive control). Next, CD3-activated T cells were incorporated with 3H-Thymidine and added to the cultures for 16 h. Following, proliferation of the T cells, a known marker for their activation^[25,26] was assessed and normalized to the response of the cells to the naïve tissue. As shown, significantly lower proliferation was detected with cells exposed to the decellularized human tissues (Figure 2d). As expected, differences between the immune responses of the different donors were detected, indicating on a possible advantage of a personalized treatment (Figure 2e).

We next sought to evaluate the immune response to the biomaterials *in vivo*. Decellularized omenta from pigs, FVB mice or C57 black mice were implanted on the omentum of C57 black mice to evaluate the xenogeneic, allogeneic, and autologous implant effect, respectively (Figure S4, Supporting Information). Recently, it was reported that reactive oxygen species (ROS) production by leukocytes is considered a sensitive parameter for inflammation, and may even predict the degree of biomaterial/patient compliance.^[27] Therefore, 7 days postimplantation, the endogenously produced hydrogen peroxide was imaged by intraperitoneal injection of a chemiluminescent luminophore, which can specifically identify the molecule.^[28] As shown, compared to the xenogeneic material, significantly lower ROS production was observed in both the autologous and allogeneic materials (Figure 2f,g). The levels of ROS production after autologous material implantation were lower than the allogeneic material, but did not reach significance. This may be attributed to the low variations between ECM proteins of different mice strains.

A major challenge in the field of tissue engineering is how to directly differentiate cells in large, 3D microenvironments for the formation of thick, functional tissues. In tissue engineering, iPSCs are usually differentiated first on monolayers of MG and then transferred to the scaffold of choice. However, direct differentiation within the scaffolding material would benefit from cell–cell and cell–matrix interactions throughout development and maturation. Here, stromal cells from the omentum, which were reprogrammed with OCT4, KLF4, c-MYC, and SOX2 to become iPSCs, according to the method described by Takahashi and Yamanaka,^[9] were mixed with the

omentum hydrogel solution in high concentration. The mixture was heated to 37 °C to crosslink the 3D hydrogel. The iPSCs were homogeneously distributed within the hydrogel and remained proliferating pluripotent stem cells in culture for at least two weeks, as judged by the expression of OCT4 and KI67 markers (Figure 3a). These undifferentiated cellular constructs were termed “day 0 implants”.

In order to explore the potential of the hydrogel to support cellular differentiation, we exposed the thick, 3D, day 0 implants to distinct differentiation protocols toward mesodermal lineages, such as the cardiac, endothelial and adipogenic, and neuroectodermal lineages, such as the cortical, dopaminergic, and spinal cord.^[29–33] Such tissue implants are useful for treating diseases in which cell death occurs and tissue function is lost. For example, myocardial infarction results from blockage of one of the coronary arteries that supply blood to the cardiac tissue, leading to ischemia of a segment of the heart. This ischemic process eventually leads to the death of contractile cells and the formation of scar tissue.^[34] Since cardiomyocytes cannot proliferate, and the number of stem cells in the heart is limited, the cardiac tissue is unable to regenerate, leading to chronic cardiac dysfunction and eventually to heart failure. Engineered heart patches have been developed to promote regeneration of infarcted cardiac tissues.^[35–39] Here, we hypothesized that our approach can be used to engineer personalized cardiac tissues. Day 0 implants were exposed to a cardiac lineage differentiation protocol, as described previously.^[29] As shown in Figure 3b, the majority of the cells that were present in day 15 implants expressed NKX2-5, an early marker for cardiac progenitor cells. Moreover, the cells highly expressed troponin T (TNNT2), sarcomeric actinin, and connexin 43 (CX43), which are late-stage proteins that are associated with contraction and electro coupling and indicating on the maturation of the cardiac implant (Figure 3b,c). Although MG is not approved for clinical studies due to its tumorigenic source, it remains an important substrate for culturing iPSCs during differentiation.^[40] Therefore, we investigated the efficiency of cellular differentiation within our implants and compared to differentiation on MG. Immunostaining results were supported by fluorescent-activated cell sorting (FACS) analysis, revealing that, for implants that were made using our approach, over 90% of the cells expressed NKX2-5, with a similar TNNT2 expression. Such TNNT2 expression is significantly higher than in the MG culture (Figure 3d; Figure S5, Supporting Information). RNA sequencing revealed high enrichment of transcripts involved in contractility (Figure 3e). Furthermore, the cells within the 3D implants developed into electrically active, functional cardiac tissues (Figure 3f), generating strong contractions that resulted in movement of the entire implant with a longitude change of $18.35 \pm 3.320 \mu\text{m}$. Implants of up to 1 cm in size were formed by this approach and showed contractility (Movie S1, Supporting Information). The tissue was responsive to external electrical stimuli (Movies S2 and S3, Supporting Information) and a conduction velocity of up to 8.57 cm s^{-1} was recorded (Figure S6, Supporting Information). Previously, it was shown that more advanced maturation of such cardiac implants may be achieved by exposing them to physical conditioning with increasing intensity over time.^[41]

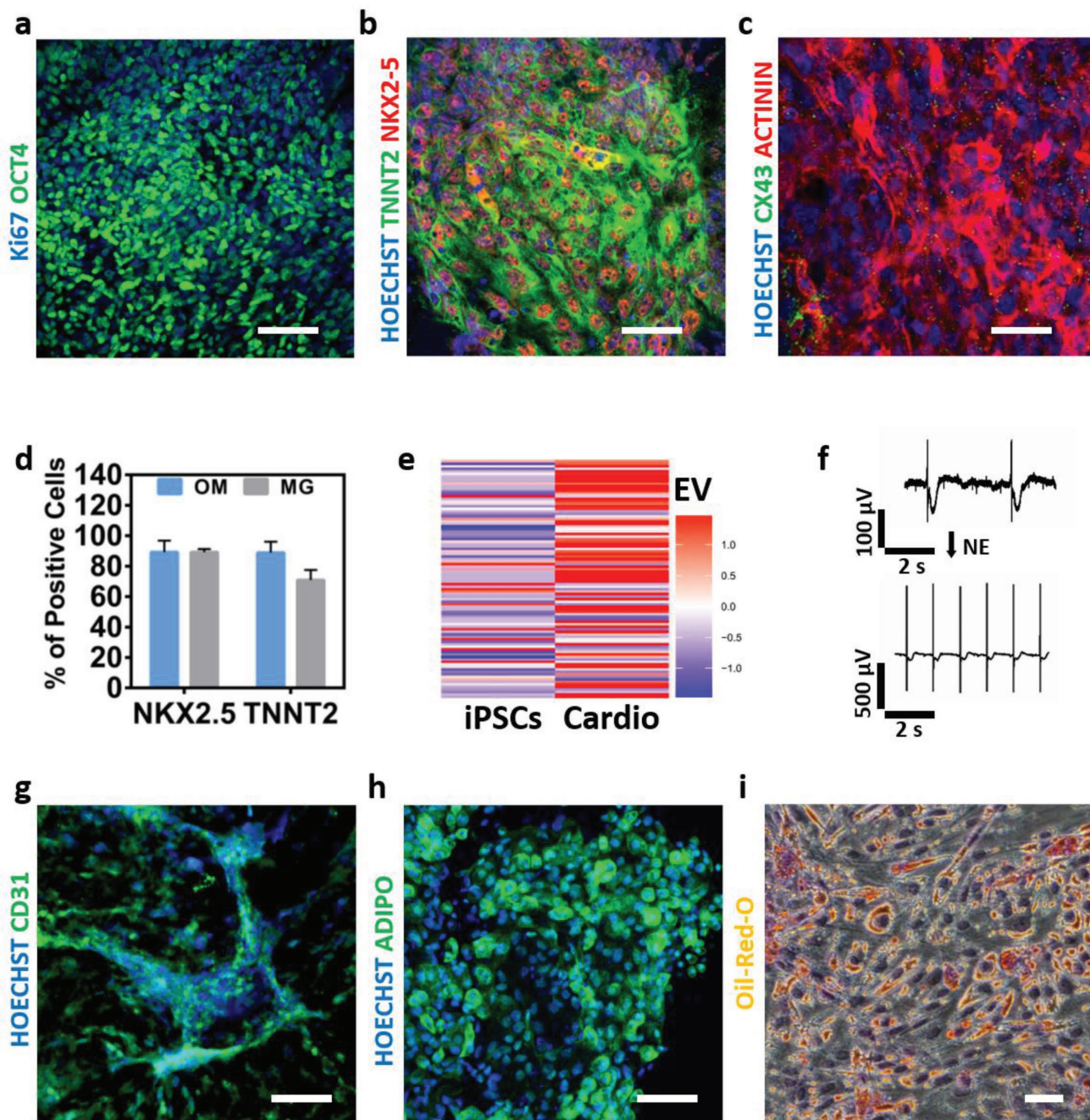


Figure 3. Engineered cardiac, endothelial and adipogenic implants. a) Immunostaining of encapsulated undifferentiated iPSC after 14 days in culture (blue: Ki67, green: OCT4). b–f) Differentiation to cardiac lineage. (b) Staining for NKX2-5 (red), TNNT2 (green), and nuclei (blue). (c) Staining for actinin (red) CX43 (green) and nuclei (blue). (d) FACS analysis of cardiac differentiation (NKX2-5 and TNNT2) in omentum hydrogel (blue) or MG (gray) on day 15. (e) A heatmap of expression of genes associated with contraction of cardiac muscle. iPSCs indicates day 0 undifferentiated iPSCs in the omentum hydrogel. Cardio indicates iPSCs-derived cardiac cells on day 30 in the omentum hydrogel. EV– Expression value. Gene list is available in Table S1 of the Supporting Information. (f) Electrical activity of cardiac implants before and after administering norepinephrine. g) Differentiation to endothelial cells as judged by CD31 staining (green). h) Adipocyte differentiation within the implant by adiponectin (green) and i) Oil-Red-O staining for lipids. Scale bars = 50 μ m. (c) = 25 μ m, (i) = 100 μ m. All experiments were performed with three different iPSCs lines and at least three biological replicates.

Endothelial cell (EC) differentiation is essential for vascularization, which improves the probability of efficient engraftment following transplantation.^[42] Therefore, we next evaluated the potential of the hydrogel to support EC differentiation. iPSCs were

subjected to an EC differentiation protocol for seven days, and CD31 expression was then assessed (Figure 3g). FACS analyses showed that the hydrogel was beneficial for EC differentiation, similar to the MG culture (Figure S7, Supporting Information).

We next sought to demonstrate that the hydrogel supports the differentiation of other mesodermal tissues. Thus, the potential of day 0 implants to serve as a fatty tissue filler following cosmetic procedures, biopsies or surgeries was investigated. On day 28, postinduction of the adipocyte differentiation protocol, the cells highly expressed adiponectin (Figure 3h) and the entire tissue exhibited high lipid content (Figure 3i), indicating the successful engineering of a fatty tissue implant. No difference was found between the high differentiation efficiency achieved in the hydrogel and the MG (Figure S8, Supporting Information). Similar to engineered cardiac tissues, neuronal implants may be used to treat diseases or injuries that are associated with the CNS, including brain lesions caused by

physical injury or neurodegenerative disease, and spinal cord injuries.^[43] To demonstrate the versatility of our approach, the cells in the 3D hydrogel were exposed to protocols that induced differentiation to cortical, dopaminergic, and spinal cord motor neurons. The cells were initially differentiated to deep cortical layer neurons^[31] and organized as 3D multilayer structures (Figure S9, Supporting Information), expressing high levels of β 3 tubulin (TUJ1), an early general marker for neurons (Figure 4a). Moreover, the cells exhibited pronounced T-box brain 1 (TBR1) expression, associated with cortical layers 1, 5, and 6 that include intercortical neurons (Figure 4a). The implants expressed the mature neuronal markers microtubule-associated protein 2 (MAP2), synaptophysin (SYP), and

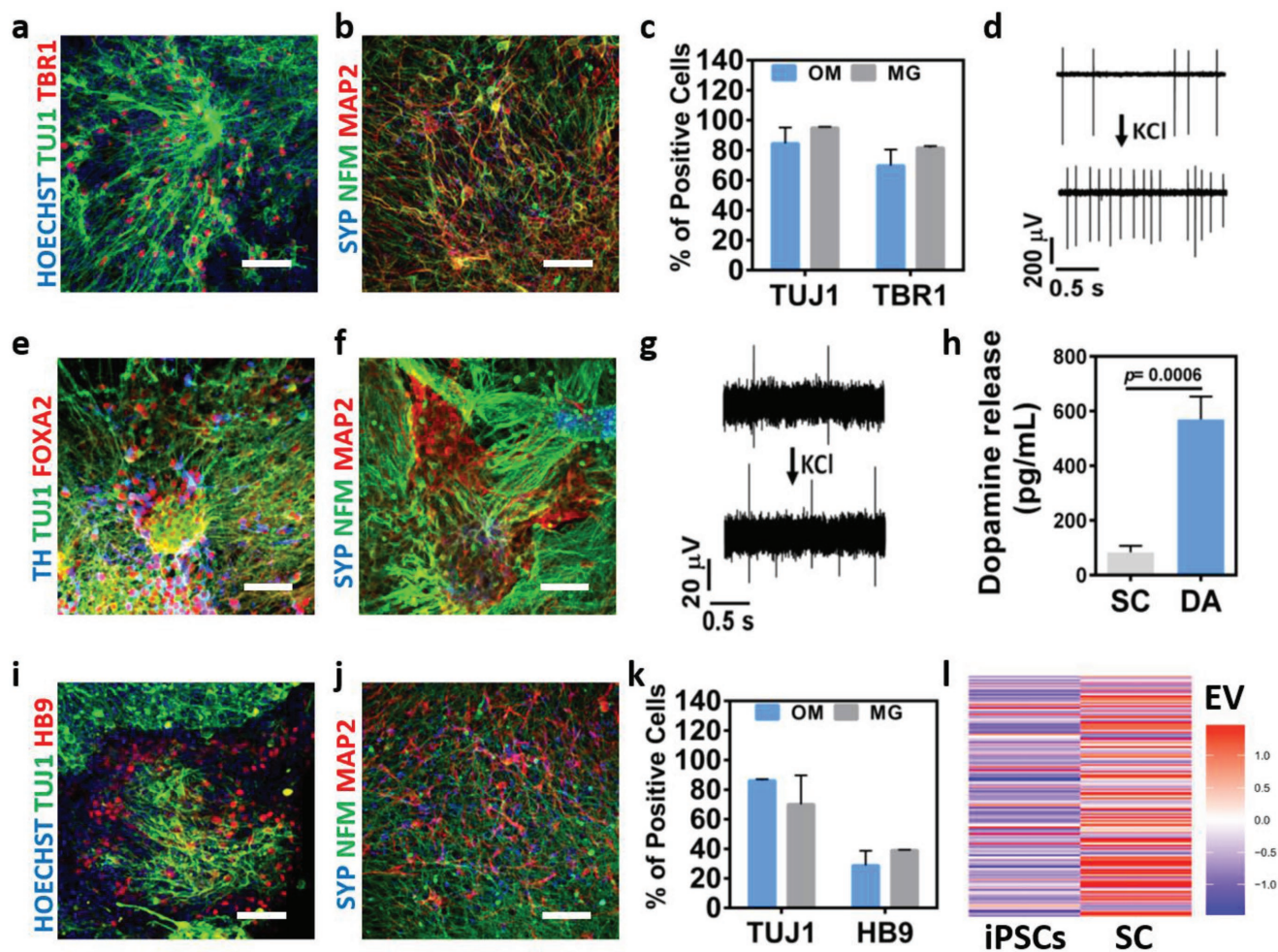


Figure 4. Engineered cortical, dopaminergic and spinal cord motor implants. a–d) Engineering cortical implants. (a) Cortical implants were stained for TBR1 (red), TUJ1 (green), and nuclei (blue). (b) Staining for MAP2 (red), NFM (green), and SYP (blue) to observe formation of synapses. (c) FACS analysis of cortex differentiation (TUJ1 and TBR) in omentum hydrogel (blue) or MG (gray) on day 30. (d) Electrical activity within the cortical implants before and after administrating KCl. e–h) Engineering dopaminergic implants. (e) Dopaminergic neurons were stained for FOXA2 (red), TH (blue), and TUJ1 (green). (f) Staining for MAP2 (red), NFM (green), and SYP (blue) to observe maturation of neuronal networks. (g) Electrical activity within the dopaminergic implants before and after administrating KCl. (h) Secretion of dopamine measured by ELISA. The released amount is compared between secretion by spinal cord (SC) neurons and dopaminergic neurons (DA). i–k) Engineering spinal cord implants. (i,j) Immunostaining of motor neurons for HB9 (red), TUJ1 (green), and nuclei (blue). (j) Staining for MAP2 (red), NFM (green), and SYP (blue) to observe formation of synapses. (k) FACS analysis of motor neurons (TUJ1 and HB9) in omentum hydrogel (blue) or MG (gray) on day 30. l) A heatmap of expression of genes associated with secretion of neurotransmitters. iPSCs indicates day 0 undifferentiated iPSCs in the omentum hydrogel. SC indicates iPSCs-derived spinal cord motor neurons on day 30 in the omentum hydrogel. EV – Expression value. Gene list is available in Table S1 of the Supporting Information. All scale bars = 50 μ m. All experiments were performed with three different iPSCs lines and at least three biological replicates.

neurofilament (NFM) (Figure 4b). Quantification of FACS analyses showed the TBR1 expression within the tissue implants to be at the same level of the MG-induced neurons (Figure 4c; Figure S10, Supporting Information), indicating on the efficiency of the differentiation within the hydrogel. In addition, the cortical neurons within the implants exhibited synaptic activity (Figure 4d; Movie S4, Supporting Information). In the same manner, implants of dopaminergic neurons expressing forkhead box protein A2 (FOXA2), tyrosine hydroxylase (TH) and TUJ1 (Figure 4e), and the mature markers (Figure 4f), revealed electrical activity (Figure 4g), dopamine release (Figure 4h), and spontaneous signal propagation (Movie S5, Supporting Information).

Recently, the potential of neuronal treatment for regenerating injured spinal cord was reported.^[44] In order to engineer patient-specific motor neuron implants, the cell-containing hydrogels were exposed to a differentiation protocol that included dual SMAD inhibition, retinoic acid and purmorphamine.^[30] The cells assembled into neuronal networks with multiple intertwined motor neurons (Figure 4i) and synapses (Figure 4j), as judged by expression of the homeobox gene HB9, and colocalization of MAP2, NFM, and SYP. Quantification of FACS analyses revealed that the hydrogel was able to efficiently support cell differentiation, similar to the MG culture (Figure 4k; Figure S11, Supporting Information). Moreover, RNA sequencing revealed the potential of the implants to secrete neurotransmitters (Figure 4l).

Overall, no traces of OCT4 staining could be observed in all lineages, indicating on a very efficient differentiation (Figure S12, Supporting Information). Although the hydrogels used for differentiation to the different lineages had similar initial stiffness, we have noticed alteration of the mechanical properties throughout the differentiation period (Figure S13, Supporting Information). Moreover, fiber orientation was altered by the cells during culture according to their fate (Figure S14, Supporting Information). Such alterations of the hydrogel stiffness, and remodeling and alignment of the ECM fibers are essential for proper cell differentiation and function.^[45,46]

Dissecting some of the functional genetic networks that govern developmental functions revealed in most cases a clear advantage to differentiation within the omentum hydrogel, as compared to MG (Figure S15, Supporting Information). These enriched networks and tissue-specific genes (Figure S16, Supporting Information) exemplified the potential of the hydrogel to direct proper differentiation into the desired tissue lineage, allowing the engineering of functional patient-specific tissues.

Here, we have demonstrated that different types of personalized tissue implants can be engineered from one small biopsy of an individual. We show that compared to the widely used xenogeneic materials, autologous materials provoke significantly lower immune response. The patient-specific hydrogel provides an appropriate, biocompatible support for self-renewal of pluripotent stem cells that originate from the same initial tissue extract. The hydrogel's 3D microenvironment supports an efficient differentiation of cells to desired lineages, and encourages physiological processes that are necessary for tissue assembly, development, and maturation. Although iPSCs are considered a promising strategy for obtaining an autologous source of cardiac and neuronal cells, there are still safety issues,

such as their genomic instabilities and their ability to induce tumor formation, that must be addressed before their use in the clinic.^[47,48] We believe that the reported concept, where the matrix and the cells are taken from the omentum of the patient paves the way for the use of personalized implants with reduced immune response, therefore, may provide better conditions for engraftment.

Experimental Section

Omentum Hydrogel Formation: Omentum Decellularization: Human omenta (informed consent was obtained from each individual patient - the request was approved by the "Assaf Harofeh Medical Center" Israel ethical committee, protocol number – Helsinki #0237-16-ASF), or omenta from the remains of healthy pigs (Kibutz Lahav – designated for the food industry) were washed with phosphate buffered saline (PBS). Then, moved to hypotonic buffer (10×10^{-3} M Tris, 5×10^{-3} M ethylenediamine tetraacetic acid (EDTA), and 1×10^{-6} M phenylmethanesulfonyl-fluoride, pH 8.0) for 1 h. Next, tissues were frozen and thawed three times using the same buffer. The tissues were washed gradually with 70% ethanol and 100% ethanol for 30 min each. Lipids were extracted by three, 30 min washes of 100% acetone, followed by 24 h incubation in a 60/40 (v/v) hexane: acetone solution (three changes). The defatted tissue was washed in 100% ethanol for 30 min and incubated overnight at 4 °C in 70% ethanol. Then, the tissue was washed four times with PBS (pH 7.4) and incubated in 0.25% Trypsin-EDTA (Biological Industries) O.N. The tissue was washed thoroughly with PBS and incubated with 1.5 M NaCl for 24 h (three changes), followed by washing in 50×10^{-3} M Tris (pH 8.0), 1% triton-X100 (Sigma) solution for 1 h. The decellularized tissue was washed in PBS followed by double distilled water and then frozen (–20 °C) and lyophilized.

Solubilized Omentum Hydrogel: After lyophilization, decellularized omentum was ground into powder (Wiley Mini-Mill, Thomas Scientific, Swedesboro, NJ, USA). Dry, milled omentum was enzymatically digested for 96 h, at RT with stirring, in a 1 mg mL⁻¹ solution of pepsin (Sigma, 4000 U mg⁻¹) in 0.1 M HCl. Subsequently, pH was adjusted to 7.4 using either DMEM/F12 $\times 10$ or PBS X10 (Biological industries). The final concentration of decellularized omentum in the titrated solution was either 1% or 1.5% (w/v). At least six human and ten pig omenta were used.

Immune Response In Vitro Assay: Decellularized human and pig omenta were digested with collagenase type II (95 U mL⁻¹, Worthington, Lakewood, NJ, USA) in PBS (37 °C, overnight). Human peripheral blood mononuclear cells (PBMCs) were isolated from three healthy adult donors (following informed consent; Helsinki #0237-16-ASF) by standard density centrifugation using Ficoll-Paque PLUS (GE Healthcare, Little Chalfont, UK). Subsequently, interface PBMCs were harvested, washed three times with cold PBS and counted.

The isolation of monocytes and macrophages was performed by MACS technology using the Human CD14 Microbead isolation kit according to manufacturer's instructions (Miltenyi Biotec, Bergisch Gladbach, Germany). B cells were isolated from the unbound fraction (which contain all lymphocyte and NK cells) using the CD19 Microbead isolation kit according to manufacturer's instructions (Miltenyi Biotec). All cells were grown in RPMI 1640 supplemented with 10% v/v inactivated human serum. Monocytes, macrophages and B cells were incubated with the digested omenta samples for 48 h at 37 °C. T cells (originated from the unbound fraction of the CD19 isolation kit) were incubated for 48 h in RPMI only and subsequent activation overnight using anti-CD3 Ab (10 µg mL⁻¹, Abcam, Cambridge, MA, USA). The activated T cells were added to the samples (containing monocytes, macrophages, B cells, and digested omenta) and incubated for 16 h following addition of 3H-Thymidine (PerkinElmer, Welltham, MA, USA). Cell proliferation was monitored by following 3H-Thymidine Incorporation using the TRI-CARB beta scintillation counter (Canberra Packard). Results were normalized to negative control samples with no digested omenta (containing only monocytes, macrophages, and B cells), for each donor. Normalized data were normalized again to positive control samples (containing

monocytes, macrophages, B cells, and digested pig naïve omenta), for each donor. A consent was obtained from all human donors.

Immune Response In Vivo: Omenta from pigs, FVB mice or C57BL mice were decellularized as described above and subsequently implanted on the omentum of C57 black mice (each omenta implant weighed ≈ 1 mg). At day 7 postimplantation the mice were anaesthetized by subcutaneously injecting with ketamine (100 mg kg^{-1}) and xylazine (10 mg kg^{-1}) in saline solution. The mice were then injected intraperitoneally with $100 \mu\text{L}$ of chemiluminescent luminophore at a concentration of $100 \times 10^{-3} \text{ M}$ in PBS (0.1% DMSO) and immediately placed in a BioSpace Lab PhotonIMAGER (Bio space lab, France). The images were taken 14 min after the injection and analyzed using M3Vision software. Photon intensity images were set to a min of 1.65×10^1 and of max of 1.84×10^1 and then quantified for the area of photon signal using imageJ software (NIH).

All mice were treated according to ethical regulations of Tel Aviv University. Permission was granted by the ethical committee, protocol number 04-18-002 - "Testing the Immune Response to Decellularized Tissue Implantation into the Peritoneum Cavity".

Multielectrode Array Measurements: A high-resolution microelectrode array recording system (Multichannel Systems, Reutlingen, Germany) was used to characterize the electrophysiological properties of the implants. Data were acquired by measuring signals using a ME64-FAI-MPA-System (Multichannel systems). Data were visualized using MC Rack software (Multichannel systems) and acquired at a sample rate of 10 kHz. Norepinephrine bitartrate at a final concentration of $100 \times 10^{-9} \text{ M}$ (Sigma-Aldrich) was used to increase cardiomyocyte beating rate, and $40 \times 10^{-3} \text{ M}$ KCL was used to excite neuronal samples. Electrical signal was measured from at least three different 3D implants, which were gently presses onto the electrode array.

Stimulation was performed using a Multichannel systems ADPT-EcoFlexMEA36-STIM adapter and an STG-4002 stimulus generator (Multichannel systems). Pacing was performed by applying 1–5.5 V, 50 ms long pulses at 1–2 Hz. Data were obtained from at least three implants.

Statistical Analysis: Statistical analysis data are presented as means \pm s.d. Differences between samples were assessed by student's *t*-test. $p < 0.05$ was considered significant. ns denotes not significant. Analyses were performed using GraphPad Prism version 6.00 for Windows (GraphPad Software).

Other methods can be found in the Supporting Information: rheological analysis, culturing undifferentiated iPSCs, multilineage induction, cell coculture, cell isolation from the omentum implants/matrigel, immunostaining, confocal imaging and FACS, viability assay, and scanning electron microscopy.

Supporting Information

Supporting Information is available from the Wiley Online Library or from the author.

Acknowledgements

R.E., I.G., and N.N. contributed equally to this work. R.E. was supported by Tel Aviv University Center for Nanoscience and Nanotechnology. T.D. received support from European Research Council Starting Grant 637943, the Slezak Foundation, the Israeli Science Foundation (700/13), the Israel Ministry of Science, Technology and Space (3-12587), and Moxie Foundation. The authors would like to thank Dr. Rivka Ofir from Ben-Gurion University, Israel, for generating and supplying the human omentum iPSCs.

Conflict of Interest

The authors declare no conflict of interest.

Keywords

autologous, decellularized hydrogels, induced pluripotent stem cells, non-immunogenic, tissue engineering

Received: June 19, 2018

Revised: August 27, 2018

Published online:

- [1] T. Dvir, B. P. Timko, D. S. Kohane, R. Langer, *Nat. Nanotechnol.* **2011**, *6*, 13.
- [2] B. P. Chan, K. W. Leong, *Eur. Spine J.* **2008**, *17*, 467.
- [3] B. N. Brown, S. F. Badylak, *Transl. Res.* **2014**, *163*, 268.
- [4] J. L. Ferrara, J. E. Levine, P. Reddy, E. Holler, *Lancet* **2009**, *373*, 1550.
- [5] S. F. Badylak, T. W. Gilbert, *Semin. Immunol.* **2008**, *20*, 109.
- [6] K. Wiles, J. M. Fishman, P. De Coppi, M. A. Birchall, *Tissue Eng., Part B* **2016**, *22*, 208.
- [7] A. Lynn, I. Yannas, W. Bonfield, *J. Biomed. Mater. Res.* **2004**, *71B*, 343.
- [8] M. Vadori, E. Cozzi, *Tissue Antigens* **2015**, *86*, 239.
- [9] K. Takahashi, S. Yamanaka, *Cell* **2006**, *126*, 663.
- [10] S. Sances, L. I. Bruijn, S. Chandran, K. Eggan, R. Ho, J. R. Klim, M. R. Livesey, E. Lowry, J. D. Macklis, D. Rushton, C. Sadegh, D. Sareen, H. Wichterle, S. C. Zhang, C. N. Svendsen, *Nat. Neurosci.* **2016**, *19*, 542.
- [11] Y. Avior, I. Sagi, N. Benvenisty, *Nat. Rev. Mol. Cell Biol.* **2016**, *17*, 170.
- [12] R. S. Mahla, *Int. J. Cell Biol.* **2016**, *2016*, 1.
- [13] D. Steiner, H. Khaner, M. Cohen, S. Even-Ram, Y. Gil, P. Itsykson, T. Turetsky, M. Idelson, E. Aizenman, R. Ram, Y. Berman-Zaken, B. Reubinoff, *Nat. Biotechnol.* **2010**, *28*, 361.
- [14] M. A. Lancaster, M. Renner, C. A. Martin, D. Wenzel, L. S. Bicknell, M. E. Hurles, T. Homfray, J. M. Penninger, A. P. Jackson, J. A. Knoblich, *Nature* **2013**, *501*, 373.
- [15] K. C. Murphy, S. Y. Fang, J. K. Leach, *Cell Tissue Res.* **2014**, *357*, 91.
- [16] S. Yamaguchi, R. Morizane, K. Homma, T. Monkawa, S. Suzuki, S. Fujii, M. Koda, K. Hiratsuka, M. Yamashita, T. Yoshida, S. Wakino, K. Hayashi, J. Sasaki, S. Hori, H. Itoh, *Sci. Rep.* **2016**, *6*, 38353.
- [17] F. Mannello, G. A. Tonti, *Stem Cells* **2007**, *25*, 1603.
- [18] E. L. Shelton, S. D. Poole, J. Reese, D. M. Bader, *J. Tissue Eng. Regener. Med.* **2013**, *7*, 421.
- [19] H. Zaha, S. Inamine, *Surg. Endosc.* **2010**, *24*, 103.
- [20] M. Shevach, R. Zax, A. Abrahamov, S. Fleischer, A. Shapira, T. Dvir, *Biomed. Mater.* **2015**, *10*, 034106.
- [21] J. Rosenblatt, B. Devereux, D. G. Wallace, *J. Appl. Polym. Sci.* **1993**, *50*, 953.
- [22] N. Soffer-Tsur, D. Peer, T. Dvir, *J. Controlled Release* **2017**, *257*, 84.
- [23] U. Galili, S. Shohet, E. Kobrin, C. Stults, B. Macher, *J. Biol. Chem.* **1988**, *263*, 17755.
- [24] Y. K. Lin, D. C. Liu, *Food Chem.* **2006**, *99*, 244.
- [25] D. Peer, P. Zhu, C. V. Carman, J. Lieberman, M. Shimaoka, *Proc. Natl. Acad. Sci. USA* **2007**, *104*, 4095.
- [26] D. Peer, E. J. Park, Y. Morishita, C. V. Carman, M. Shimaoka, *Science* **2008**, *319*, 627.
- [27] N. Bryan, H. Ashwin, N. Smart, Y. Bayon, N. Scarborough, J. A. Hunt, *Biomaterials* **2012**, *33*, 6380.
- [28] O. Green, S. Gnaim, R. Blau, A. Eldar-Boock, R. Satchi-Fainaro, D. Shabat, *J. Am. Chem. Soc.* **2017**, *139*, 13243.
- [29] X. Lian, C. Hsiao, G. Wilson, K. Zhu, L. B. Hazeltine, S. M. Azarin, K. K. Raval, J. Zhang, T. J. Kamp, S. P. Palecek, *Proc. Natl. Acad. Sci. USA* **2012**, *109*, E1848.

- [30] D. Shimojo, K. Onodera, Y. Doi-Torii, Y. Ishihara, C. Hattori, Y. Miwa, S. Tanaka, R. Okada, M. Ohyama, M. Shoji, A. Nakanishi, M. Doyu, H. Okano, Y. Okada, *Mol. Brain* **2015**, *8*, 79.
- [31] R. Edri, Y. Yaffe, M. J. Ziller, N. Mutukula, R. Volkman, E. David, J. Jacob-Hirsch, H. Malcov, C. Levy, G. Rechavi, I. Gat-Viks, A. Meissner, Y. Elkabetz, *Nat. Commun.* **2015**, *6*, 6500.
- [32] C. Patsch, L. Challet-Meylan, E. C. Thoma, E. Urich, T. Heckel, J. F. O'Sullivan, S. J. Grainger, F. G. Kapp, L. Sun, K. Christensen, Y. Xia, M. H. Florido, W. He, W. Pan, M. Prummer, C. R. Warren, R. Jakob-Roetne, U. Certa, R. Jagasia, P. O. Freskgard, I. Adatto, D. Kling, P. Huang, L. I. Zon, E. L. Chaikof, R. E. Gerszten, M. Graf, R. Iacone, C. A. Cowan, *Nat. Cell Biol.* **2015**, *17*, 994.
- [33] I. Cuaranta-Monroy, Z. Simandi, Z. Kolostyak, Q. M. Doan-Xuan, S. Poliska, A. Horvath, G. Nagy, Z. Bacso, L. Nagy, *Stem Cell Res.* **2014**, *13*, 88.
- [34] G. Vunjak-Novakovic, N. Tandon, A. Godier, R. Maidhof, A. Marsano, P. T. Martens, M. Radisic, *Tissue Eng., Part B* **2010**, *16*, 169.
- [35] K. R. Stevens, K. L. Kreutziger, S. K. Dupras, F. S. Korte, M. Regnier, V. Muskheli, M. B. Nourse, K. Bendixen, H. Reinecke, C. E. Murry, *Proc. Natl. Acad. Sci. USA* **2009**, *106*, 16568.
- [36] F. Weinberger, K. Breckwoldt, S. Pecha, A. Kelly, B. Geertz, J. Starbatty, T. Yorgan, K.-H. Cheng, K. Lessmann, T. Stolen, M. Scherrer-Crosbie, G. Smith, H. Reichensperner, A. Hansen, T. Eschenhagen, *Sci. Transl. Med.* **2016**, *8*, 363ra148.
- [37] T. Dvir, A. Kedem, E. Ruvinov, O. Levy, I. Freeman, N. Landa, R. Holbova, M. S. Feinberg, S. Dror, Y. Etzion, J. Leor, S. Cohen, *Proc. Natl. Acad. Sci. USA* **2009**, *106*, 14990.
- [38] A. F. Godier-Furnémont, T. P. Martens, M. S. Koeckert, L. Wan, J. Parks, K. Arai, G. Zhang, B. Hudson, S. Homma, G. Vunjak-Novakovic, *Proc. Natl. Acad. Sci. USA* **2011**, *108*, 7974.
- [39] L. A. Reis, L. L. Chiu, Y. Liang, K. Hyunh, A. Momen, M. Radisic, *Acta Biomater.* **2012**, *8*, 1022.
- [40] L. G. Villa-Diaz, A. M. Ross, J. Lahann, P. H. Krebsbach, *Stem Cells* **2013**, *31*, 1.
- [41] K. Ronaldson-Bouchard, S. P. Ma, K. Yeager, T. Chen, L. Song, D. Sirabella, K. Morikawa, D. Teles, M. Yazawa, G. Vunjak-Novakovic, *Nature* **2018**, *1*, 239.
- [42] B. Wang, S. S. Patnaik, B. Brazile, J. R. Butler, A. Claude, G. Zhang, J. Guan, Y. Hong, J. Liao, *Crit. Rev. Biomed. Eng.* **2015**, *43*, 455.
- [43] I. Elliott Donaghue, R. Tam, M. V. Sefton, M. S. Shoichet, *J. Controlled Release* **2014**, *190*, 219.
- [44] Z. Anna, J.-W. Katarzyna, C. Joanna, M. Barczewska, W. Joanna, M. Wojciech, *Stem Cells Int.* **2017**, *2017*, 3978595.
- [45] C. M. Madl, B. L. LeSavage, R. E. Dewi, C. B. Dinh, R. S. Stowers, M. Khariton, K. J. Lampe, D. Nguyen, O. Chaudhuri, A. Enejder, S. C. Heilshorn, *Nat. Mater.* **2017**, *16*, 1233.
- [46] E. Sleep, B. D. Cosgrove, M. T. McClendon, A. T. Preslar, C. H. Chen, M. H. Sangji, C. M. R. Perez, R. D. Haynes, T. J. Meade, H. M. Blau, S. I. Stupp, *Proc. Natl. Acad. Sci. USA* **2017**, *114*, E7919.
- [47] J. J. Cunningham, T. M. Ulbright, M. F. Pera, L. H. Looijenga, *Nat. Biotechnol.* **2012**, *30*, 849.
- [48] A. Guhr, S. Kobold, S. Seltmann, A. E. S. Wulczyn, A. Kurtz, P. Löser, *Stem Cell Rep.* **2018**, *11*, 485.